Materials Today Communications 38 (2024) 107983

Contents lists available at ScienceDirect

Materials Today Communications

journal homepage: www.elsevier.com/locate/mtcomm

Corrosion behaviour of electropolished magnesium materials

Jessica Kloiber [a,b], Ulrich Schultheiß [a], Lamborghini Sotelo [c,d], George Sarau [c,e,f], Silke Christiansen [c,e,g], Sarkis Gavras [h], Norbert Hort [h,i], Helga Hornberger [a,b,*]

[a] Biomaterials Laboratory, Faculty of Mechanical Engineering, Ostbayerische Technische Hochschule (OTH), Seybothstraße 2, 93053 Regensburg, Germany
[b] Regensburg Center of Biomedical Engineering (RCBE), Ostbayerische Technische Hochschule (OTH), Seybothstraße 2, 93053 Regensburg, Germany
[c] Institute for Nanotechnology and Correlative Microscopy eV (INAM), Äußere Nürnberger Str. 62, 91301 Forchheim, Germany
[d] Friedrich–Alexander University Erlangen–Nürnberg (FAU), Staudtstraße 7, 91058 Erlangen, Germany
[e] Fraunhofer Institute for Ceramic Technologies and Systems (IKTS), Äußere Nürnberger Str. 62, 91301 Forchheim, Germany
[f] Max Planck Institute for the Science of Light, Staudtstr. 2, 91058 Erlangen, Germany
[g] Freie Universität Berlin, Arnimallee 14, 14195 Berlin, Germany
[h] Helmholtz-Zentrum Hereon, Max-Planck-Straße 1, 21502 Geesthacht, Germany
[i] Institute of Product Technology and Systems, Leuphana University Lüneburg, Universitätsallee 1, 21335 Lüneburg, Germany

ARTICLE INFO

Keywords:
Magnesium alloy
Pure magnesium
Electropolishing
Corrosion behaviour
Surface characterisation
Biomedical application

ABSTRACT

Although magnesium and its alloys are promising candidates as biodegradable implant materials, the tendency for localised corrosion mechanism in physiological environment limit their biomedical application. Electropolishing is an attractive strategy for improving the corrosion behaviour of metals, but it is still largely unexplored in magnesium materials. In this study, the characterisation of electropolished surfaces of AM50 and pure magnesium was performed, focussing on their in vitro degradation behaviour in cell medium. Corrosion rates were evaluated using potentiodynamic polarisation. The surface morphology before and after the onset of corrosion was investigated by scanning electron microscopy and confocal laser scanning microscopy. The presented electropolishing process led to improved surface performances, observable by significantly lower corrosion rates (0.08 mm·year^{-1} in Dulbecco's modified Eagle's medium), lower arithmetical mean height (0.05 μm), lower water contact angle (25–35°) and lower micro hardness (35–50 HV 0.1) compared to mechanically and chemically treated surfaces. MgO/$Mg(OH)_2$ could be detected on electropolished surfaces. The localised corrosion mode could be reduced, but not entirely prevented. Electropolishing shows great potential as post-treatment of magnesium-based components, but detailed tests of the long-term corrosion behaviour are an important area of future research.

1. Introduction

In recent years, magnesium and its alloys have attracted considerable attention in the biomedical field due to several properties that make them promising candidates as biodegradable materials in temporary implant applications [1,2]. The main advantage, compared to conventional inert metals, is the unique combination of biocompatibility, resorbability and mechanical stability [3–5]. Magnesium-based implants are expected to provide mechanical support at local damaged places in the body and corrode completely after the tissue has healed, avoiding the need for a second surgical procedure [2,4]. Since magnesium is an essential mineral in the human body, a controlled release of

Abbreviation: MGri, mechanical grinding; MPol, mechanical polishing; EPol, electrochemical polishing; CPick, chemical pickling; TEM, transmission electron microscopy; HAADF STEM, high-angle annular dark-field scanning transmission electron micrographs; EDS, energy-dispersive X-ray detector; FIB, focussed ion beam; SCE, saturated calomel electrode; DMEM, Dulbecco's Modified Eagle's Medium; FBS, fetal bovine serum; CR, corrosion rate; CLSM, confocal laserscanning microscopy; SEM, secondary electron microscopy; SFE, surface free energy; SE, secondary electron; BSE, back-scattered electron; COMPO, composition; TOPO, topography; XPS, X-ray photoelectron spectroscopy.

* Corresponding author at: Biomaterials Laboratory, Fac ulty of Mechanical Engineering, Ostbayerische Technische Hochschule (OTH), Seybothstraße 2, 93053 Regensburg, Germany.

E-mail addresses: jessica.kloiber@oth-regensburg.de (J. Kloiber), ulrich.schultheiss@oth-regensburg.de (U. Schultheiß), sotelo.lamborghini@gmail.com (L. Sotelo), george.sarau@ikts.fraunhofer.de (G. Sarau), schrist1@gwdg.de (S. Christiansen), sarkis.gavras@hereon.de (S. Gavras), norbert.hort@hereon.de (N. Hort), helga.hornberger@oth-regensburg.de (H. Hornberger).

https://doi.org/10.1016/j.mtcomm.2023.107983
Received 22 August 2023; Received in revised form 5 December 2023; Accepted 26 December 2023
Available online 28 December 2023

magnesium ions from degrading implants is generally uncritical [6,7]. In fact, magnesium materials are said to offer a stimulating effect on tissue and bone regeneration [7–9]. Considering the mechanical properties of the metal, magnesium and its alloys are favourable for load bearing applications because density and elastic modulus are very similar to those of natural bone [1,10]. For all these reasons, magnesium materials have mainly been investigated for the use in tissue engineering as scaffolds [11,12] as well as for orthopaedic and cardiovascular applications as screws, plates and stents [13–15].

However, the widespread application of magnesium and its alloys as temporary implant material has not been established yet [1], as magnesium materials exhibit a high corrosion rate as well as strong tendency for localised corrosion mechanism in physiological environment. This may lead to a premature loss of mechanical integrity and consequently to failure of magnesium-based implants before tissue healing is completed [4,10,16]. In general, the most common corrosion types of magnesium and its alloys are galvanic and pitting corrosion. Especially factors, such as impurities, secondary phases or intermetallic compounds in the material [3,17] as well as the presence of chloride ions in the human body fluid [4] can reduce the corrosion resistance significantly. In addition, a fast and uncontrolled degradation of magnesium is accompanied by intense hydrogen evolution as well as local increase of pH in the surrounding tissue [6,18]. Therefore, one of the greatest challenges in the development of magnesium-based implants is the control of the corrosion rate [7].

In principle, there are two common strategies to control the degradation of magnesium materials: (i) metallurgical modification to optimise the composition and microstructure through alloying [3] or appropriate manufacturing methods [2], and (ii) surface modification to alter surface features by preparing protective surface coatings or performing surface treatments [15,19]. Among these strategies, surface treatments are an attractive method to improve the corrosion behaviour of magnesium materials because the surface of an implant material is the first contact partner with human body fluid. In recent years, mainly mechanical, chemical or physical techniques have been studied intensively [3,15,19,20], although electrochemical treatments, such as electropolishing, offer a versatile alternative.

Electropolishing, also called electrochemical polishing, electrolytic polishing or anodic polishing, is a material removal process. It is based on anodic dissolution, which removes the material ion by ion from the metal or alloy surface [21,22]. A classic electropolishing system consists of an electrochemical cell, including an anode and a cathode electrode in an electrolyte solution. The workpiece to be polished works as anode (+) and the tool electrode is utilised as cathode (-). When a direct current voltage is applied, current flows from the anode to the cathode whereby the metal on the workpiece surface dissolves in the electrolyte based on an electrolysis process and a new oxide layer is formed [21,23]. Generally, electropolished surfaces are characterised by a reduction in roughness, residual stresses and non-metallic inclusions as well as by an improved protective passive oxide layer [24,25]. These are all factors which lead to the main benefit of an increased corrosion resistance. Furthermore, it is a contact-free process which makes it suitable for workpieces with small dimensions and complex geometries [21,26]. Consequently, it is already a common method for the surface finishing of surgical instruments as well as medical implants made of metals [21,27,28]. Due to the poor surface integrity in the as-built state, electropolishing also provides good prospects for the post-processing of additively manufactured components [29].

So far, however, most research in electropolishing has been carried out on stainless steel [23,27]. Regarding magnesium materials, there is no industrially established process publicly known [27]. A mixture of mineral acids and alcohols, mostly phosphoric acid and ethanol in a ratio of 3:5 (v/v), is mentioned to be a suitable electrolyte solution [7,30,31]. Additionally, it can be noted that electropolishing of magnesium materials is carried out at room temperature [30] or 0 °C [32] in a voltage range of 1–3 V [7,30–32]. The polishing time varies between 20 and 120 s [7,30,32]. The setting of other relevant parameters is not mentioned. Besides the lack of an established electropolishing process for magnesium materials, there is also too little information to what extent the treatment can optimise the surface properties of this resorbable metal.

The aim of this study was to develop an appropriate electropolishing process for magnesium materials without using toxic components and to characterise the electropolished surfaces. The focus of the present characterisation was the investigation of the corrosion behaviour, but also changes of other surface features, such as wettability or hardness, were studied. Even electropolishing of magnesium material is already in industrial use, for example in the production of stents, however, there is still a lack of knowledge about the resulting surface properties and their optimisation. Traditional electropolishing electrolytes are often accompanied by toxic elements, which may leave a contamination risk for medical application, even when careful cleaning processes after electropolishing are applied. In summary, the study was targeted to advance the electropolishing as a suitable method for post-treatments of magnesium-based components.

2. Materials and methods

2.1. Surface treatments

Magnesium sheet AM50 was selected as working material in the present study. It is not a metallic biomaterial, but a common and readily available magnesium material. Therefore, it has been used as an example of a magnesium alloy for basic demonstration purposes. The raw material was provided by the Helmholtz-Zentrum Hereon in Geesthacht, Germany. In addition, the measurements were carried out on pure magnesium sheet (99,98 wt% Mg; HWM Hauner GmbH), which served as a reference material. The sheets were approximately 1 mm thick and were cut into small samples with a dimension of 25 × 10 mm.

To evaluate the effects of electropolishing on the surface properties of the samples, the electrochemical method was compared with three alternative post-treatments: two mechanical procedures, mechanical grinding (MGri[1]) and mechanical polishing (MPol[2]), as well as a chemical pickling (CPick[3]) process.

2.1.1. Mechanical grinding (MGri) and polishing (MPol)

To prepare mechanically treated surfaces, specimens of AM50 and pure magnesium were mechanically ground by a series of P240, P600, P1200 and P2500 SiC papers. The grinding process was carried out using ethanol (94 vol%) instead of water due to the high reactivity of magnesium materials with aqueous solutions. After each grinding step, the samples were cleaned with ethanol (94 vol%) and dried with a blow-dryer. This method was also used as pre-treatment for all specimens in this study to ensure uniform surface conditions and experiment reproducibility. In addition to the mechanically ground (MGri) samples, further samples of AM50 and pure magnesium were ground to P4000 grit size, which served as mechanically polished (MPol) specimens.

2.1.2. Electrochemical polishing (EPol[3])

For the electropolishing treatment, the area of the sample was first limited to a defined size of 1 cm^2 with a shrink tube. The electrochemical process was carried out in an electrolyte solution composed of concentrated phosphoric acid (85 vol%), ethanol (99 vol%) and deionized water in a ratio of 40:55:5 (v/v). The experimental setup of electropolishing is shown in Fig. 1.

The magnesium materials were used as anode (+) while stainless steel 1.4301 was utilised as cathode (-). The electrolyte was kept at room temperature (20–23 °C) and the distance between the counter and working electrode was fixed at 30 mm. Furthermore, an Ag/AgCl (in 3 M KCl) reference electrode has been included in the setup to measure the current density vs. potential curve of the system. For the electrochemical treatment of both magnesium materials, a voltage of 4 V

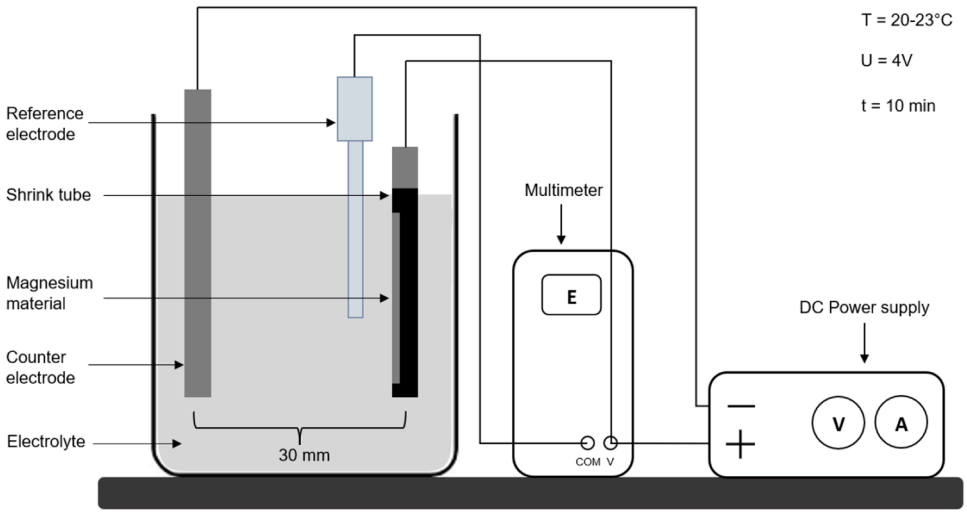

Fig. 1. Schematic illustration of the experimental setup of electropolishing.

within the active region was chosen. Successful electropolishing was assessed by the physical appearance of the treated surfaces, and preliminary investigations showed that shiny surfaces could already be generated in a low voltage range. Electropolishing was then carried out for 10 min per sample with an immersed anode to cathode area of 1:4. The electropolishing parameters are summarised in Table 1.

Since magnesium materials are already attacked by the electrolyte solution in the currentless state [27], the anode was immersed in the electrolyte when voltage was applied. After electrochemical polishing, the specimens were rinsed in deionized water and cleaned with ethanol (94 vol%) before drying.

2.1.3. Chemical pickling (CPick[4])

For the third type of surface treatment, the samples were completely immersed in a beaker filled with 20 wt% citric acid for 5 min. The acid solution temperature was kept at room temperature (20–23 °C). After the pickling, the specimens were cleaned with deionized water and ethanol (94 vol%) to remove all residues of the acid treatment.

2.2. Transmission electron microscopy (TEM[5])

TEM micrographs were obtained to investigate the microstructure of the AM50 alloy. A Thermo Fisher F200i TEM at an acceleration voltage of 200 kV was used to obtain high-angle annular dark-field scanning transmission electron micrographs (HAADF STEM[6]). The TEM was also equipped with a Bruker Super-Twin energy-dispersive X-ray detector (EDS[7]) which was used to elementally map regions within the samples. The TEM specimens were prepared via focussed ion beam (FIB[8]) using a TESCAN Lyra3 FIB-SEM. The samples were ion milled to a thickness of approximately 100 nm and an electron transparent region of approximately 10 × 10 μm.

2.3. Optical microscopy

For further microstructure analysis, samples of AM50 and pure magnesium were embedded in acrylic resin. After several grinding processes with SiC paper up to P2500, the specimens were polished with 3 μm and 1 μm diamond suspension. The final polishing was carried out with colloidal silica suspension (0.03 μm). In the last step, the embedded samples were etched in nital. The macro- and microstructure of the magnesium materials was visualised with the optical microscope BX51 (Olympus).

2.4. Electrochemical analysis

Electrochemical measurements were performed to evaluate the corrosion behaviour of the different surface-treated specimens. In this context, potentiodynamic polarisation was carried out with the mini-cell system (Ibendorf & Co.GmbH) which consists of a platinum counter electrode, a saturated calomel reference electrode (SCE[9]) and a working electrode. The tests were realised at room temperature with the cell medium Dulbecco's Modified Eagle Medium (DMEM[10]) (SH30585.02, Merck). The composition of the electrolyte is shown in Table 2.

For some selected measurements, 10 wt% fetal bovine serum (FBS[11]) (S181B; Biowest) and 1 wt% Antibiotic-Antimycotic (L0010; Biowest) were added to DMEM. The sample's area exposed to the electrolyte solution was 0.008 cm^2. With the potentiostat PGSTAT204 (Metrohm), a potential range between −0.3 V and 1.5 V and a scan rate of 0.01 V/s was set. The analysis of the resulting data was performed by using the software NOVA 2.1 (Metrohm). For each sample, three measuring points were examined. The polarisation resistance R_p was determined at the

Table 2
Concentrations of ions and components of the electrolyte DMEM.

Ion or component	Unit	DMEM
Na^+	mmol/l	154.5
K^+	mmol/l	5.4
Mg^{2+}	mmol/l	0.8
Ca^{2+}	mmol/l	1.8
Cl^-	mmol/l	118.5
HCO_3^-	mmol/l	44.0
HPO_4^{2-}	mmol/l	0.9
SO_4^{2-}	mmol/l	0.8
Amino acids	g/l	1.6
Glucose	g/l	4.5

DMEM: Dulbecco's Modified Eagle's Medium

Table 1
Relevant process parameters for electropolishing of magnesium materials.

Electropolishing parameter	Voltage [V]	Current density [A/cm^2]	Polishing time [min]	Electrolyte temperature [°C]	Electrode distance [mm]
Value	4	0.03	10	20-23	30

corrosion potential E_{corr} ± 30 mV. For the calculation of the current corrosion density i_{corr}, the Tafel constants were adjusted to 0.12 V/dec.

Thus, the corrosion rate (CR[12]) was calculated according to ASTM G102–23:

$$CR = K_1 \bullet \frac{i_{corr}}{\rho} \quad EW \tag{1}$$

where CR is given in mm/year, i_{corr} in μA/cm^2 and $K_1 = 3.27 \cdot 10^{-3} \frac{mm \bullet g}{\mu A \bullet cm \bullet year}$.

The variable equivalent weight EW was determined by calculation. For pure magnesium, EW is given by:

$$EW = \frac{W}{n} \tag{2}$$

where W = the atomic weight of magnesium and n = the number of electrons required to oxidise an atom of magnesium.

For the alloy AM50, EW was determined as follows:

$$EW = \frac{1}{\sum \frac{nifi}{Wi}} \tag{3}$$

where ni = the valence of the ith element of the alloy, fi = the mass fraction of the ith element of the alloy and Wi = the atomic weight of the ith element in the alloy.

The density ρ was also calculated for both materials. For AM50 and pure magnesium, the variables result in the following values:

$EW_{AM50} = 11.950$, $EW_{Mg} = 12.153$,

$\rho_{AM50} = 1.780$ g·cm^{-3}, $\rho_{Mg} = 1.738$ g·cm^{-3}.

2.5. Confocal laser-scanning-microscopy (CLSM[13])

The confocal laser scanning microscope LEXT4000 (Olympus) was used for a precise evaluation of the surface quality of magnesium materials after the different surface finishes. For the analysis of the surface roughness, the calculation of the arithmetical mean height S_a and the maximum height S_z was carried out at a cut-off wavelength λ of 80 μm and an area of approx. 1 cm^2. S_a is defined as an absolute value that describes the difference in height of each point compared to the arithmetical mean of the surface while S_z indicates the sum of the largest peak height value and the largest pit depth value within a defined area. Three measurement points were selected for each sample and a mean value was calculated for both roughness parameters. For the categorisation of surface defects, defined as pits in the surface, three measurements of the depth and diameter were taken and averaged. The surface-treated samples were also analysed after the onset of corrosion to evaluate the changed surface roughness qualitatively.

2.6. Scanning electron microscopy (SEM[14])

SEM micrographs were used to investigate the surface morphology of the different treated magnesium materials. In this context, the scanning electron microscope Leo 1455VP (Carl Zeiss AG) at an acceleration voltage of 20 kV was used. The working distance were set to 20 mm. The device also includes an EDS system, which enables the determination of the elemental composition of the bulk material. Additionally, corroded areas of surface-treated samples, after contact with the cell medium DMEM, were analysed.

2.7. Raman spectroscopy

The Raman LabRam NANO HR800 spectrometer (Horiba Scientific) was used to measure the surface composition of AM50 and pure magnesium samples after the different surface treatments. Measurements were carried under ambient conditions using a 50x objective, an excitation wavelength of 532 nm, and a grating of 300 nm. Laser power was set to 60 mW with an exposure time of 5 s and 2 accumulations to ensure a good noise/signal ratio while preventing laser damage to the sample. In order to obtain statistically significant spectra, at least 20 points were measured on each sample and an average spectrum was calculated.

2.8. Contact angle measurements

To study the wetting behaviour of the various surface-treated specimens, the Drop Shape Analyzer DSA25 (Krüss GmbH) with the software ADVANCE was used. Static contact angle and surface free energy of the magnesium materials were measured at room temperature with ultrapure water and diiodomethane (2 μl drop volume). For some selected measurements of the contact angle, DMEM with 10 wt% FBS and 1 wt% Antibiotic-Antimycotic was used as test liquid. The contact angle was measured immediately after the contact between the drop and the specimen's surface to minimise evaporation. Three measurement points were selected for each sample and a mean value of the contact angle was determined. The surface free energy (SFE[15]) was calculated according to Owens and Wendt model:

$$\sigma_{SL} = \sigma_S + \sigma_L - 2\sqrt{\sigma_S^d \sigma_L^d} - 2\sqrt{\sigma_S^p \sigma_L^p} \tag{4}$$

where σ_S and σ_L are the surface free energy of solid and liquid, σ_S^d and σ_L^d are dispersive components, and σ_S^p and σ_L^p are polar components of the surface free energy of solid and liquid.

2.9. Hardness measurements

The effects of the different surface treatments on the hardness of the magnesium samples were investigated at the microscopic level. Therefore, the Vickers hardness testing method was selected. The measurements were carried out with the microhardness tester Durimet (Leitz GmbH), which is equipped with an optical measuring setup. Two different test loads (HV 1 and HV 0.1) were used. For each sample, three measurements were performed at different areas of the treated surfaces. The value of the Vickers hardness was taken from the corresponding hardness tables based on the determined diagonal lengths. An average value of the microhardness was then calculated.

3. Results

3.1. Bulk microstructure and composition

The microstructure of AM50 and pure magnesium was investigated. In this context, Fig. 2(a) shows the micrograph of the magnesium alloy.

The metallographic examination by optical microscopy revealed that black point-shaped irregularities are visible on the entire surface of the AM50 samples. CLSM measurements determined that these black spots protrude from the surface with an average height of 3 μm and a diameter between 1 μm and 5 μm. As shown in Fig. 3(a), TEM micrographs display these irregularities on the AM50 surface as white contrast points. A corresponding EDS mapping of these particles (Fig. 3b) indicated that these irregularities exhibit a high concentration of the alloying elements Al and Mn, while the amount of Mg is clearly reduced at these areas. This can be recognised by the accumulation or lack of colour points in the EDS maps. On the remaining surface, however, a largely uniform distribution of Mg, Al and Mn can be observed. Thus, in addition to the primary α-Mg phase, the microstructure of AM50 is characterised by inclusions or intermetallic Al-Mn-phases located both near the grain boundaries and within the matrix.

For comparison, Fig. 2(b) depicts the micrograph of pure magnesium. The material exhibits a high density of twins in the grains, which might be the result of the rolling process during sheet production. In addition, small black particles are found on the surface of the magnesium sample, mainly distributed along the grain boundaries. According

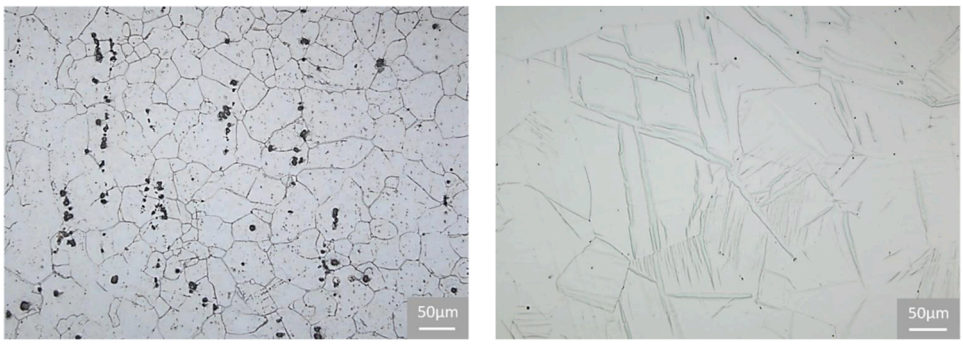

Fig. 2. Optical microscopy pictures of (a) AM50 and (b) pure magnesium. The inclusions of AM50 (visible as black spots) are located near the grain boundaries and within the matrix. Pure magnesium exhibits a high density of twins in the grains and impurities (visible as small black spots) along the grain boundaries.

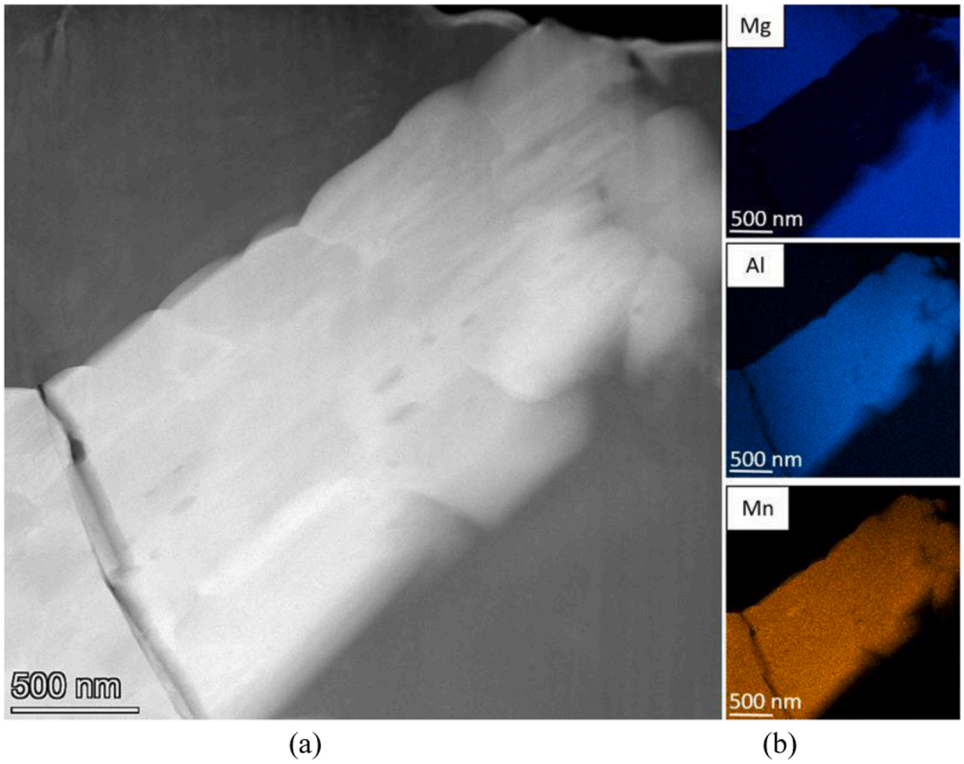

Fig. 3. HAADF-STEM micrograph of AM50 (a) and EDS mapping of magnesium, aluminium, and manganese at the same surface area (b). The inclusions on the surface, visible as white spots in the TEM picture, correlate with low magnesium and high aluminium and manganese concentrations.

to the manufacturer's specification of a purity of 99.98%, it can be assumed that these spots are manufacturing-related impurities.

3.2. Surface composition

In order to be able to determine and compare the changed surface composition of AM50 and pure magnesium after the different surface treatments, corresponding Raman spectra in the range of 100–3000 cm^{-1} were measured and the results are given in Fig. 4.

It is obvious that the treated surfaces show four low intensity bands at around 820 cm^{-1}, 890 cm^{-1}, 1560 cm^{-1} and 2330 cm^{-1}. These peaks can be attributed to vibrations of O_2 and N_2 or other contaminations on the surface [33], due to the measurement on ambient air. Regarding the ground AM50 sample, the surface exhibits a peak at around 1000–1100 cm^{-1}. Singh et al. [34] associated second order Raman bands of MgO with this peak. Since a magnesium oxide layer formed in air was already present before the mechanical treatment, it may have been completely removed by grinding but rebuilt after grinding in ambient air. In contrast, the pickling treatment leads to two noticeable peaks centred at 1330 cm^{-1} and 1600 cm^{-1}, which are characteristic of carbonaceous materials [35]. Since the electrolyte of the pickling treatment consisted of citric acid, these intense bands can be associated with the adsorption of citrate on the chemically-treated surface [36].

The Raman spectra of electropolished samples of AM50 and pure magnesium show no significant difference. Both electropolished materials also exhibit a peak at about 1000–1100 cm^{-1}, which, in addition to MgO residuals, may be PO_4^{3-} residuals [37], due to the used electropolishing electrolyte, consisting of phosphoric acid. In this context, also $Mg_3(PO_4)_2$ [38,39] is conceivable as the dissolved magnesium ions may have reacted with the phosphoric acid during electropolishing. Further Raman bands for both electropolished materials are observed at around 550 cm^{-1}, 1450 cm^{-1} and 2800–2900 cm^{-1}. These peaks represent MgO or $Mg(OH)_2$ [40–42] that must have formed during electropolishing. However, the peak measured on the electropolished pure

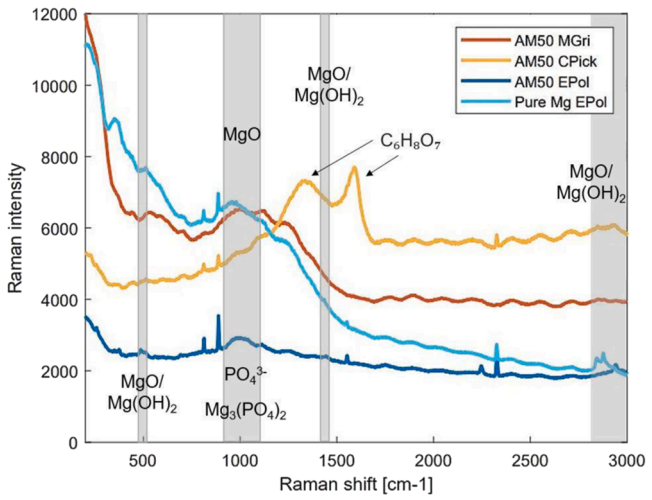

Fig. 4. Raman spectra of mechanically (orange), chemically (yellow) and electrochemically (dark blue) treated AM50 samples and an electrochemically (light blue) treated pure magnesium surface. The peaks at around 550 cm^{-1}, 1450 cm^{-1} and 2800–2900 cm^{-1} indicate that the surface of magnesium materials contains MgO/ $Mg(OH)_2$ after electropolishing.

magnesium surface at around 2800 cm^{-1} could also be a residue of ethanol [43] as the liquid was contained in the electropolishing electrolyte and used for sample cleaning.

Overall, it is evident that all examined samples exhibit residues of the respective type of surface treatment, indicating that cleaning the specimens with deionized water and ethanol cannot remove all treatment-related residues completely.

3.3. Surface morphology

A first qualitative assessment of the resulting surface quality after electropolishing is shown in Fig. 5 based on the image of an electropolished AM50 sample. It is worth noting that also magnesium materials can exhibit a shiny and mirror-like surface without any structure formation by using a parameter setting adapted to the chosen magnesium material. The gloss is a characteristic feature of electrochemically treated metal surfaces and can be attributed to micro-smoothing [44].

Moreover, the mechanism of macro-smoothing [44] can be observed after electropolishing of magnesium materials. In this context, Fig. 6 compares the resulting surface roughness of AM50 and pure magnesium after the different surface treatments. The arithmetical mean height S_a is plotted in Fig. 6(a) and the maximum height S_z in Fig. 6(b).

Fig. 6(a) shows the surface roughness as the arithmetical mean height S_a depending on the surface treatment. Thereby, CPick produced the highest S_a -values followed by MGri, MPol and EPol, the latter

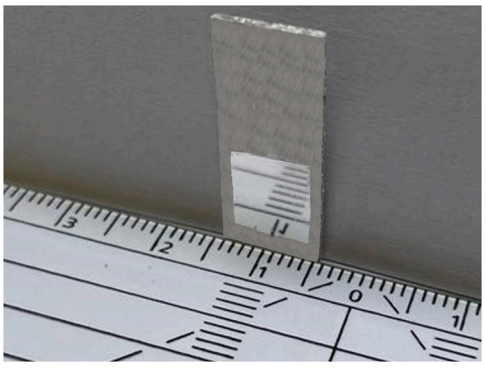

Fig. 5. Photograph of an AM50 specimen, showing a typical shiny and mirror-like surface after electropolishing, recognisable by the reflection of the ruler.

resulted in the smoothest surface independently from the material composition (AM50 or Mg). The S_a-value measuring 0.05 µm for EPol surfaces indicates a high efficiency of the electrochemical method in realising uniform and very smooth surfaces. The mechanical polished surface (EPol) achieved similar roughness values. Considering that the grinded surfaces (MGri) was the initial surface for all treatments, the S_a-values demonstrate that the pickling treatment (CPick) was roughening the surface instead of smoothening.

The roughness sequence CPick > MGri > MPol > EPol could not be observed regarding the S_z-value (Fig. 6b). Sz presents the maximum height of the surface roughness, defined as the maximum difference between the highest peak and the deepest valley. S_z-values have to be relativized by considering specific defects and waviness on the surface. For example, the comparatively high S_z range of 3–6 µm on the electropolished AM50 surface indicates some irregularities, defects or the impact of secondary phases, which have been detected in the material (Figs. 1 and 2). Significant variations between the S_z measurements of Mg and AM50 were found not only for electrochemically treated samples but also for chemically treated surfaces. Pure magnesium after EPol exhibits the lowest S_z-value (less than 1 µm) of all treatments, whereas AM50 reaches a much higher value. This indicates a largely defect-free surface of electropolished pure magnesium. As a result, the surface structure and defects of the different treated samples needs to be examined in more detail, see next chapter 3.4.

3.4. Surface defects

CLSM images depicting the surface morphology of AM50 and pure magnesium after mechanical, chemical and electrochemical treatment are shown in Fig. 7. Additionally, treatment-related surface defects were investigated and visualised with exemplary height profile measurements below the respective image. The observed defects were then categorised based on the factors shape, depth and diameter, because the measured S_z values (see chapter 3.3) were not appropriate to specify these defects.

On the ground surface of both materials (MGri), typical residues of the mechanical treatment are clearly visible in the form of parallel grinding grooves along the polishing direction on the whole surface. These irregular grinding grooves show a typical depth of about 0.6 µm. After CPick, the AM50 surface still shows slight grinding marks, indicating that the pickling time was too short. Moreover, this type of treatment has formed many round surface defects, which varies in a radius range of 5–10 µm. It should also be noted that these surface irregularities do not form pointed but extremely roundish pits with an average depth of 2.5 µm. Pickled pure magnesium, on the other hand, shows an etched surface, recognisable by visible grain boundaries.

In contrast, EPol of AM50 results in a uniform, smooth and largely structure-less surface. Besides the dark particles of the Al-Mn phases, which are still present after EPol, AM50 exhibits a few surface defects in the form of relatively flat dents. However, these defects are very difficult to see on the surface image, as these spots are not noticeably different from the rest of the surface. CLSM measurements reveal that the radius varies between 2 and 25 µm with an average depth of 1 µm, whereby a correlation between the size and the depth of the surface defects cannot be detected. Overall, electropolished AM50 has significantly less defects on the surface than the pickled one.

The studied depths of defects confirm the ranking of the Sa values in Fig. 2(a). Regarding the impact of microstructure on surface defects after electropolishing, a more uniform surface for pure magnesium than for AM50 can be noted. However, numerous very small black dots, distributed over the entire pure magnesium surface, are visible. A closer look reveals that these spots are small, pointed pits in the treated surface. With a radius of 2 µm and a depth of approx. 0.3 µm, they have only minor effect on the surface morphology. Furthermore, pure magnesium shows similar flat dents like AM50, but in a lower number.

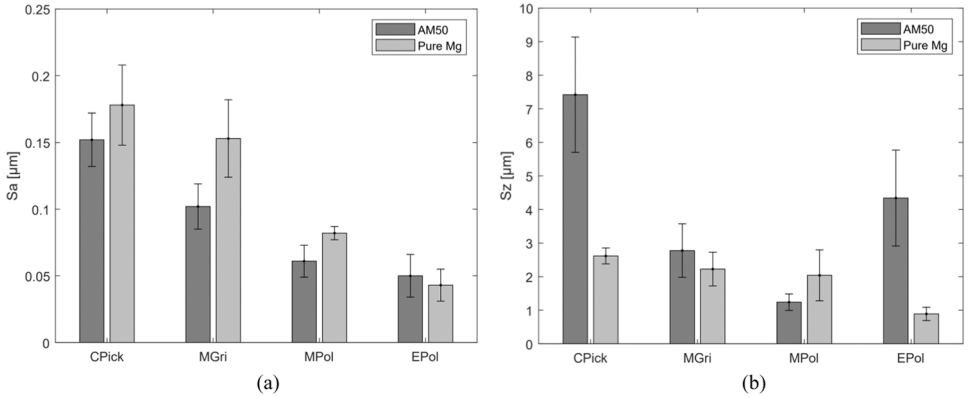

Fig. 6. Surface roughness of AM50 and pure magnesium in terms of (a) S_a and (b) S_z values after the different surface treatments. (a) Electropolishing (EPol) leads to the smoothest surface for both materials. (b) The comparatively high maximum height of AM50 indicates some irregularities on the surface. Electropolished pure magnesium exhibits the lowest S_z value of all treatments considered.

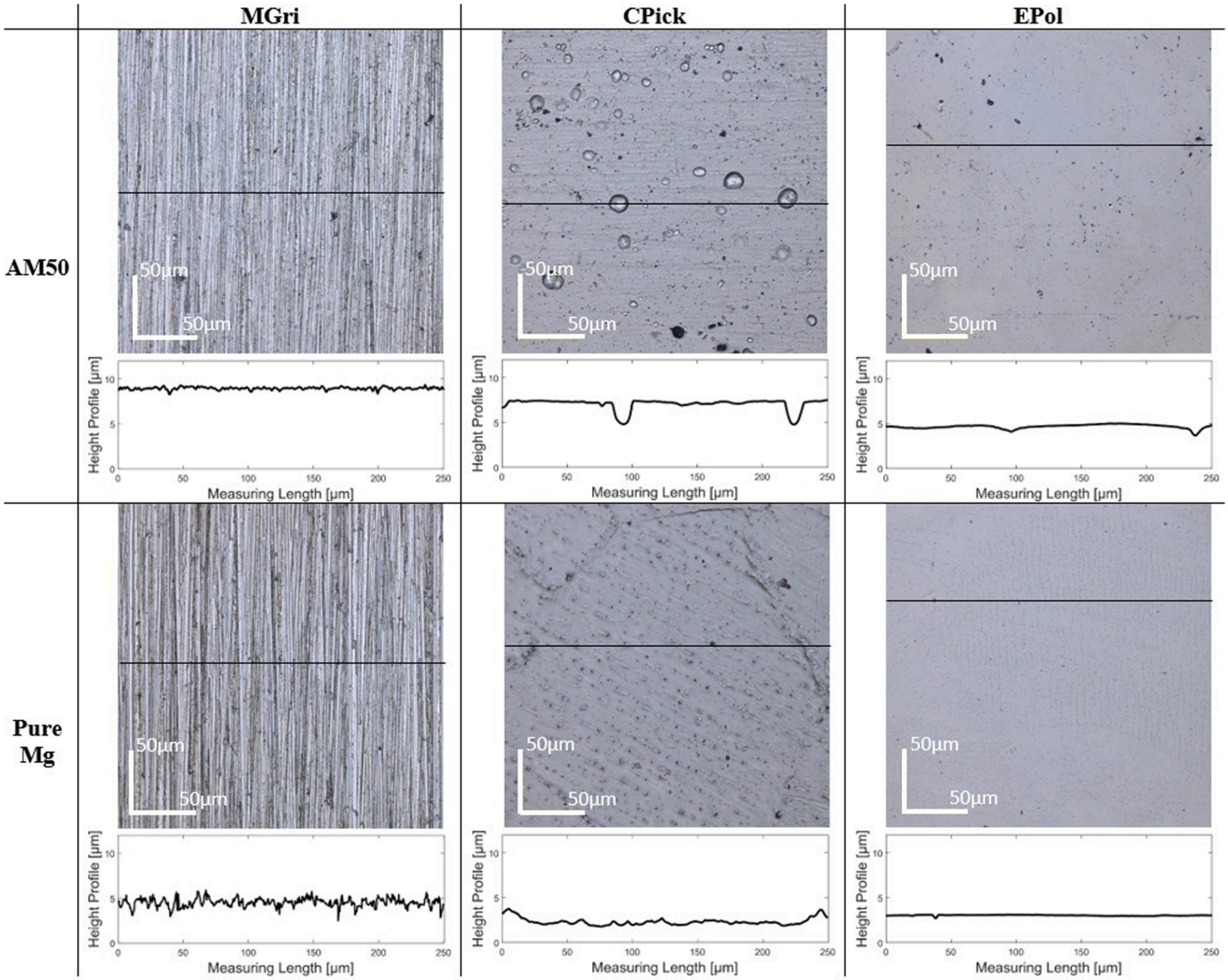

Fig. 7. Confocal Laser scanning microscopy (CLSM) images of the surface morphology of AM50 and pure magnesium after mechanical (MGri), chemical (CPick) and electrochemical (EPol) treatment. The height profile measurements of the treatment-related surface defects are plotted below the respective surface image. The electrochemical treatment of AM50 leads to some shallow surface pits while pure magnesium is largely defect-free.

3.5. Corrosion rates

The effects of electropolishing on the corrosion behaviour of magnesium materials were investigated using potentiodynamic polarisation. Polarisation curves of the different treated surfaces were measured on at least three samples and on each sample, three measurements in DMEM and three measurements in DMEM+FBS were performed. Fig. 8 depicts the resulting curves of mechanically, chemically and electrochemically treated (a) AM50 and (b) pure magnesium specimens, measured in DMEM. Of each treatment, three measurements of one sample are shown as an example; all additional examined samples showed similar behaviour and confirmed the results.

It can be observed that for both materials the type of surface treatment has a decisive influence on the level of the measured corrosion current density i_{corr}. The highest values are found after the mechanical methods MPol and MGri. The corrosion potential E_{corr} shows the most negative values. Treatment by pickling leads to a shift of the curves to a lower i_{corr} and a higher E_{corr}. However, the most significant improvement in corrosion behaviour can be observed in the electrochemically treated specimens. The polarisation curves of electropolished samples exhibit the highest E_{corr}, the lowest i_{corr} and the highest corrosion resistance R_p among all treatments considered. Moreover, it should be mentioned that despite similar arithmetical roughness values, the corrosion data of mechanically polished and electrochemically treated AM50 surfaces differ significantly. The polarisation curves of AM50 and pure magnesium show differences mainly based on E_{corr}. With around −1.7 V, the magnesium alloy indicates a value, which is 0.2 V more positive than pure magnesium. In most measurements, pure magnesium has a lower i_{corr} than AM50. However, after EPol the i_{corr} values are almost identical.

The corrosion rates calculated according to Eq. 1 (measured in DMEM) after the different surface treatments are shown, exemplified by AM50, in Fig. 9. In addition, the corrosion rates measured in the test liquid DMEM+FBS are also depicted in Fig. 9 to illustrate the influence of the chosen electrolyte.

Among all surface treatments considered, EPol leads in DMEM to the lowest corrosion rate (0.08 mm·year^{-1}) by far, indicating the formation of a more uniform and protective oxide layer. On the contrary, the chemical treatment results in a corrosion resistance that is 10 times lower than after EPol. The corrosion rates of mechanically and electrochemically treated surfaces differ by a factor of almost 20.

The addition of FBS to DMEM leads, overall, to a similar corrosion behaviour but with lower corrosion rates and less differences between the *CR* values of the various surface treatments. Although the effects of proteins on the magnesium degradation are not yet fully understood [45], the presence of a physiologically relevant mixture of proteins, contained in FBS, influences the corrosion behaviour by decreasing i_{corr}.

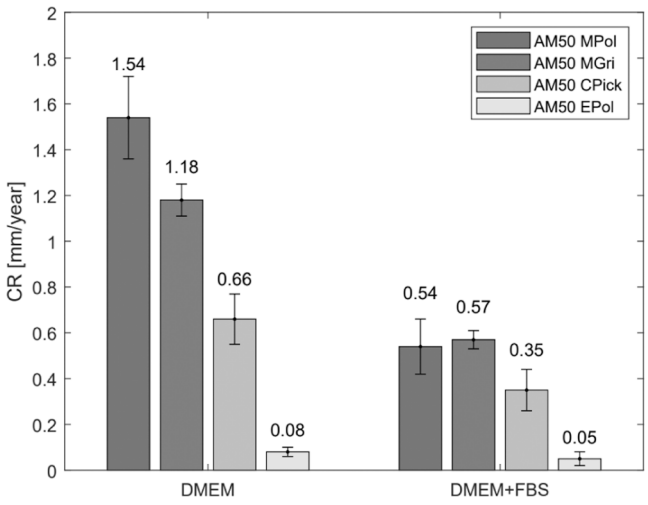

Fig. 9. Calculated corrosion rates of AM50 after the mechanical, chemical and electrochemical surface treatments, measured in the two electrolytes DMEM and DMEM+FBS. Electropolishing (EPol) results in the lowest corrosion rate (CR) of all treatments considered. While the addition of FBS leads to significantly lower CRs of mechanically and chemically treated surfaces, proteins have only minor influence on electropolished surfaces.

However, the rate of electropolished AM50 surfaces is almost identical in DMEM (0.08 mm·year^{-1}) and DMEM+FBS (0.05 mm·year^{-1}), suggesting that proteins show less impact on electrochemically treated surfaces.

Table 3 summarises all relevant electrochemical results and shows the strong influence of the chosen magnesium material, surface treatment and electrolyte on the corrosion data. For completeness, the polarisation curves of AM50 and pure magnesium (measured in DMEM+FBS) after the different surface treatments are shown in Fig. A1.

3.6. Corrosion products

After electrochemical measurements using the minicell system and the electrolyte DMEM, corroded areas on the different treated samples of AM50 and pure magnesium can be detected on the surface. In this context, Fig. 10 shows SEM images, taken with the secondary electron (SE[16]) detector, of the corrosion sites on a (a) ground, (b) pickled and (c) electropolished AM50 sample.

It is worth noting that on mechanically and chemically treated surfaces, the measuring area of the minicell is clearly visible as corroded circular area on the surface. Within this section, several pitting spots

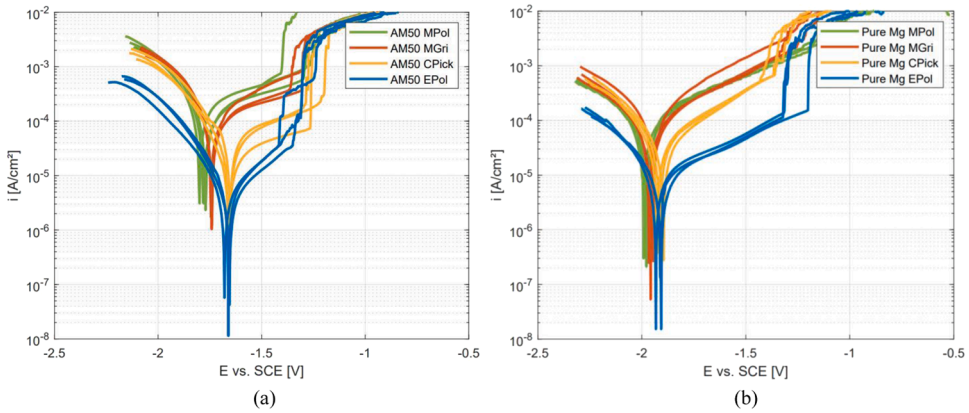

Fig. 8. Polarisation curves of a mechanically (green, orange), chemically (yellow) and electrochemically (blue) treated (a) AM50 and (b) pure magnesium sample measured in DMEM. Similar corrosion behaviour can be observed for both materials, with electropolishing (EPol) representing the surface treatment resulting in the lowest i_{corr}.

Table 3
Electrochemical data calculated from polarisation curves after the different surface treatments and electrolytes for AM50 and pure magnesium.

Material	Electrolyte	Treatment	$E_{corr\ rr}$ vs. SCE [V]	$i_{corr\ rr}$ [µA/cm^2]	R_p [Ω·cm^2]	CR [mm·year^{-1}]
AM50	DMEM	MPol	-1.73 ± 0.05	69.94 ± 26.46	440 ± 194	1.54 ± 0.18
		MGri	-1.73 ± 0.02	53.94 ± 9.35	502 ± 114	1.18 ± 0.07
		CPick	-1.69 ± 0.05	30.22 ± 16.72	1 092 ± 494	0.66 ± 0.11
		EPol	-1.66 ± 0.04	3.62 ± 1.86	9 518 ± 5 552	0.08 ± 0.02
	DMEM + 10% FBS	MPol	-1.65 ± 0.03	24.41 ± 6.81	1 151 ± 313	0.54 ± 0.12
		MGri	-1.64 ± 0.02	25.99 ± 3.59	1 029 ± 191	0.57 ± 0.04
		CPick	-1.64 ± 0.03	16.04 ± 5.83	1 880 ± 798	0.35 ± 0.09
		EPol	-1.68 ± 0.05	2.34 ± 1.74	18 270 ± 13 041	0.05 ± 0.03
pure Mg	DMEM	MPol	-1.98 ± 0.01	31.49 ± 2.34	832 ± 64	0.72 ± 0.04
		MGri	-1.95 ± 0.02	37.86 ± 14.64	790 ± 270	0.87 ± 0.25
		CPick	-1.91 ± 0.03	22.79 ± 7.17	1 230 ± 276	0.52 ± 0.05
		EPol	-1.87 ± 0.04	3.29 ± 0.89	8 634 ± 2 847	0.08 ± 0.01
	DMEM + 10% FBS	MPol	-1.96 ± 0,04	26.52 ± 6.74	1043 ± 248	0.61 ± 0.02
		MGri	-1.89 ± 0.04	19.98 ± 3.49	1 340 ± 208	0.46 ± 0.03
		CPick	-1.92 ± 0.01	18.80 ± 1.81	1 401 ± 151	0.43 ± 0.02
		EPol	-1.79 ± 0.04	1.86 ± 1.16	22 084 ± 15 618	0.04 ± 0.02

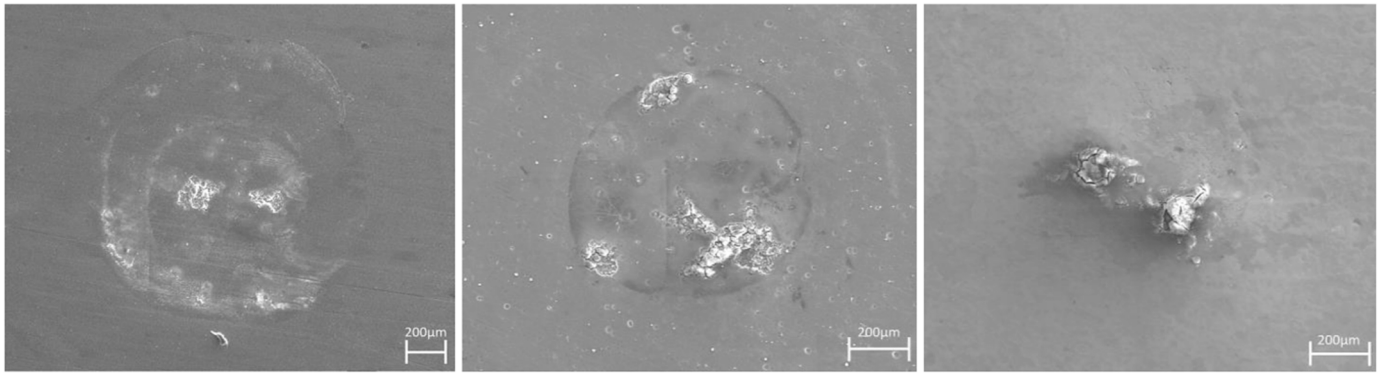

Fig. 10. Secondary electron (SE) images of the corroded areas on a (a) ground, (b) pickled and (c) electropolished AM50 surface after contact with the electrolyte DMEM. Compared to the electropolished surface, the circular area of the minicell is clearly visible on the mechanically and chemically treated surfaces, indicating lower corrosion stability in body-like fluids than electrochemically treated surfaces.

have formed. Regarding the corroded sites of electropolished AM50 samples, it should be mentioned that the measuring area of the minicell cannot be identified at all. Nevertheless, the onset of inhomogeneous corrosion can also be observed on electrochemically treated surfaces, resulting in some corrosion products on the surface. This indicates that electropolishing has not led to a change in the corrosion mechanism of magnesium materials, as pitting corrosion still occurs. However, it seems that the electrochemical treatment could slow down the superficial corrosion attack compared to the other surface treatments.

Fig. 11 gives a more detailed look at the corrosion products that formed on electropolished AM50 surfaces within the measuring area of the minicell. The SEM images were taken with the back-scattered electron (BSE[17]) detector, using the setting composition (COMPO[18]) for Fig. 11 (a) and the setting topography (TOPO[19]) for Fig. 11 (b). Typical for pitting corrosion, the corrosion process initiated at several places and spread at different rates, which can be seen in smaller and larger corrosion spots on the surface. These corrosion areas form inhomogeneous pits of 5–25 µm on the electropolished surface (Fig. 11 b). Within

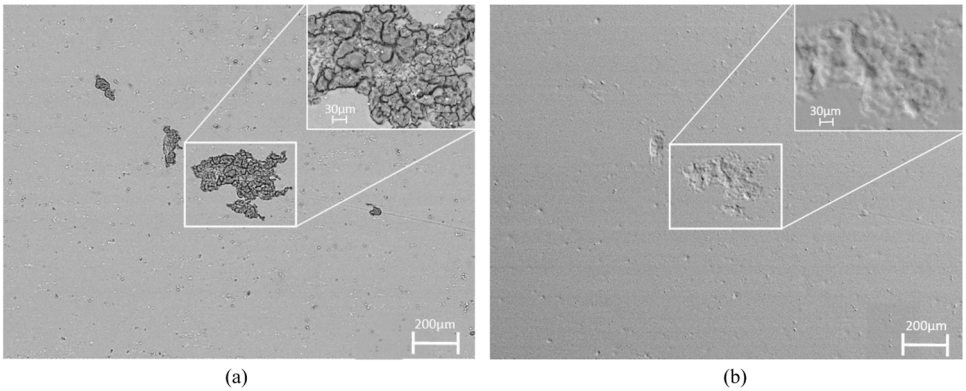

Fig. 11. (a) BSE (COMPO) image and (b) BSE (TOPO) image of the formed corrosion products on electropolished AM50 after electrochemical measurements in DMEM. The corrosion mechanism appears irregular and leads to inhomogeneous pits on the electropolished surface.

these structures, a corrosion layer of clod-like, brittle corrosion products can be observed. The inclusions or Al-Mn-phases (visible as white spots) are not removed but incorporated into the corrosion structures (Fig. 11 a). As a result, the onset of corrosion affects the surface morphology in the form of increased roughness. The S_a-value rises by a factor of 20 from 0.05 ± 0,02 µm to 1,02 ± 0,27 µm, while S_z goes up from 4,34 ± 1,43 µm to 18,42 ± 2,75 µm. Pure magnesium shows the same basic initial corrosion mechanism after electropolishing.

The elemental composition of the electropolished AM50 surface in an (a) uncorroded and (b) corroded state is compared in Fig. 12. The EDS spectra of the uncorroded area is dominated by Mg, Al, and Mn. After the onset of corrosion, the amount of Mg is reduced, whereby traces of Ca and K are detectable within the corrosion spots. Moreover, it should be noted that the corroded structures exhibit a noticeable high Cl-content. Similar composition, but without Al and Mn, are obtained for electropolished pure magnesium (Fig. A2).

3.7. Wetting behaviour

Contact angle measurements were performed to understand the wetting behaviour of magnesium surfaces after different surface treatments. In this context, Fig. 13 represents the contact angles of diiodomethane, water and DMEM+FBS measured on AM50 after MGri, MPol, CPick and EPol. In addition, the surface free energy (*SFE*) is given, which was calculated from the first two test liquids.

It can be clearly seen that the water contact angle after MGri reaches the highest observed value (approx. 80°) of all treatments considered. Hence, the surface energy exhibits the lowest value of about 40 mN/m. MPol reduces the contact angle of all three test liquids to 50–60°. Regarding CPick, a further decrease in the measured contact angles can be noted. While diiodomethane indicates a similar value to those after MGri and MPick, water achieves a contact angle of around 45°, resulting in an increased surface energy of 58 mN/m after the chemical treatment.

Nevertheless, it should be mentioned that the lowest contact angles of all test liquids can be observed after EPol. The contact angle of water drops to a value of around 30°, which is almost three times lower than after MGri. Using a body-like fluid, such as DMEM+FBS, results in contact angles similar to those of water, albeit with greater variations between the measurements. As the surface energy increases with decreasing contact angles, electropolished magnesium surfaces have the highest surface free energy of approx. 65 mN/m compared to the otherwise treated surfaces. Pure magnesium shows similar wetting properties after the different surface treatments, with a water contact angle of 36° and a surface energy of 63 mN/m after EPol (Fig. A3).

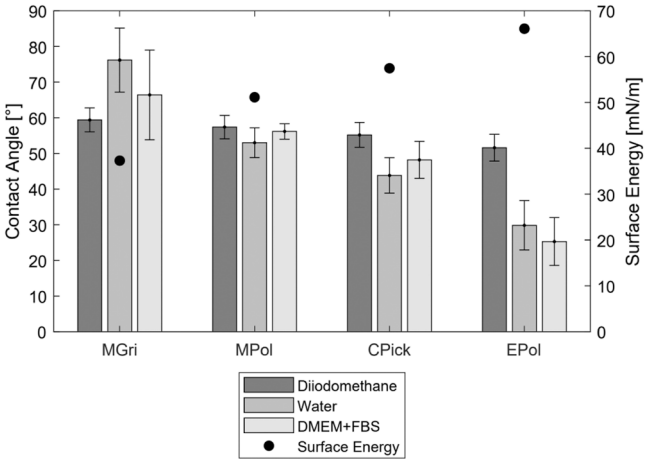

Fig. 13. Contact angles and surface energy of AM50 after mechanical grinding (MGri), mechanical polishing (MPol), chemical pickling (CPick) and electropolishing (EPol). The test liquids were diiodomethane, water and DMEM+FBS. The electrochemically treated samples indicate the best wetting behaviour while the mechanical treatments lead to relatively high contact angles and low surface energy.

3.8. Hardness

The type of the applied surface treatment can lead to changes in the hardness properties of magnesium surfaces. In this context, Fig. 14 illustrates the influence of MGri, MPol, CPick and EPol on the Vickers hardness measured for AM50 and pure magnesium at a test load of HV 0.1. Regarding AM50, the micro hardness reaches its maximum of around 80 HV 0.1 after MGri. A lower average value can be observed after CPick (approx. 70 HV 0.1). The hardness measured after MPol is comparable to that obtained after the chemical treatment, but with smaller variations between the measurements.

However, of all surface treatments considered, EPol shows the

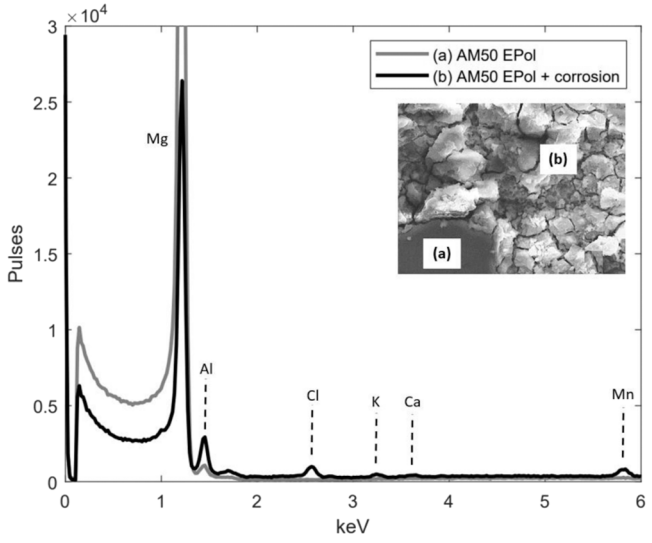

Fig. 12. EDS spectra of electropolished AM50 in the (a) uncorroded area (grey line) and (b) corroded area (black line) of the surface. Besides traces of Ca and K, an increased concentration of Cl and a decreased concentration of Mg can be detected on the AM50 surface after the onset of corrosion.

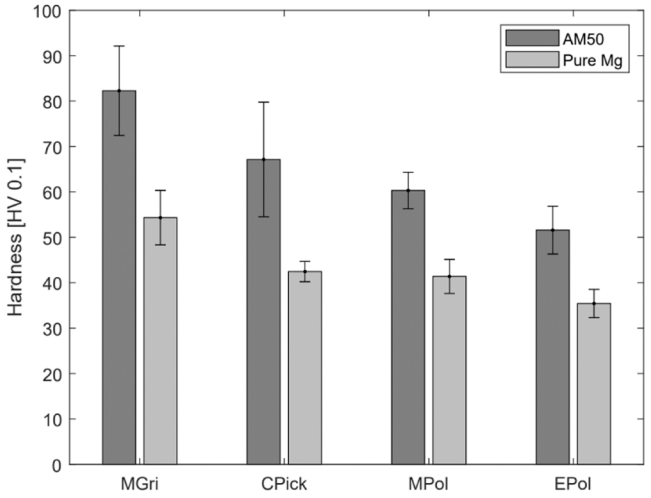

Fig. 14. Microhardness of AM50 and pure magnesium after mechanical grinding (MGri), mechanical polishing (MPol), chemical pickling (CPick) and electropolishing (EPol) at a test load of HV 0.1. Electropolished AM50 surfaces result in the greatest reduction of surface hardness, whereby mechanical and chemical treatments lead to harder surfaces. Pure magnesium shows similar behaviour after the different treatments.

greatest reduction in the surface hardness of the magnesium alloy. The electrochemical method leads to a value of approx. 50 HV 0.1. With a test load of HV 1 (Fig. A4), the differences are not as visible as with HV 0.1, as the values are all within a range of 50–60 HV 1. This could indicate that the surface layers formed after the various surface treatments are not thick enough for such a high test load, which is why the bulk material was probably measured. Pure magnesium shows similar behaviour in the determined microhardness, albeit the treatments do not differ as clearly as with AM50. Overall, the hardness of pure magnesium after EPol is about 35 HV 0.1, around 15 HV 0.1 lower than the value of the magnesium alloy.

4. Discussion

Due to its high reactivity, magnesium and its alloys are challenging for electrochemical surface treatment. In this study, the characterisation of electropolished surfaces was carried out on various magnesium materials to determine to what extent the electropolishing process can optimise the surface properties of this resorbable metal.

4.1. Electropolishing process for magnesium materials

Basically, there is only limited knowledge in the literature about how magnesium materials can be optimally electropolished. One of the most important parameters is the polishing voltage, which affects the current density of the electropolishing system. A method commonly used to determine the optimal voltage is to measure a current-density vs. potential curve [23], with the most favourable conditions for electropolishing being found in the transition area from the passive to the transpassive section [21,27]. However, for the treatment of magnesium materials a potential from the active to the passive part was chosen. It could be proven, that a typically shiny, smooth and structure-less surface is already achieved at low voltages (Fig. 5). This could be related to the reactive character of the material, resulting in a higher dissolution rate compared to standard electropolishing materials. As a result, low voltages are preferred, as a high voltage leads to high current densities during electropolishing, resulting in an undesirably high removal rate of magnesium based components [23]. Moreover, an uncontrolled formation of gas bubbles can be observed by using high voltages, which can cause structure formation and thus surface defects [27,46]. Likewise, Bahl et al. [7], Howlett et al. [30] and Hung et al. [31] used low voltages of about 1–3 V for the electropolishing of magnesium materials. Further process parameters, such as polishing time, electrolyte temperature, etc. were adjusted based on fundamental aspects of electropolishing gained over the last decades [21,23,24,27,47]. However, due to the complexity of the process and the diversity of influencing factors, optimisation strategies of the electropolishing procedure are necessary for the application on components as well as to meet the high surface demands in the biomedical field.

4.2. Microstructural influence of the magnesium material

Similar to other homogeneous materials, pure magnesium offers the best conditions for electropolishing because of the single-phase microstructure, whereby a largely uniform material removal can occur. The influence of impurities (Fig. 2) should not be underestimated, as they can promote the formation of pitting. However, the insufficient mechanical properties limit the practical application of pure magnesium [3,5]. In the case of a heterogeneous magnesium material, such as AM50, the production of an acceptable surface quality by electropolishing is more complex, as the alloying components, secondary phases, intermetallic phases or inclusions detected in the material (Figs. 2 and 3) exhibit different corrosion potentials and are normally cathodic with respect to the α-Mg matrix [10,17]. Consequently, micro-galvanic couples can form more easily, leading to inhomogeneous degradation in the form of pitting [8,11,18]. Even though AM50 is not a metallic biomaterial, it demonstrated the effects and challenges of electropolishing magnesium alloys, which are the preferred type of magnesium material in temporary implant applications [48]. Overall, the results of this study reveal that, besides the conventional electropolishing metals, also magnesium and its alloys are suitable for electropolishing by using a parameter setting adapted to the chosen material.

4.3. Electrochemical modification of the surface structure

Similar to standard electropolishing metals, also the mechanisms of anodic brightening (Fig. 5) and anodic levelling (Fig. 6) can be found for magnesium materials after electropolishing. Compared to the traditional mechanical finishing techniques, the electrochemical process removes material from a metal based on an anodic dissolution phenomenon, in which the material is removed ion by ion from the workpiece surface in a non-contact and damage-free way. Due to this special type of material removal, electropolishing stands out from the other surface treatments, resulting in a uniform, microscopically smooth (S_a = 0.05 µm) and especially structure-less surface texture. However, electropolishing of AM50 leads to comparatively high S_z values, which can be associated with the more precisely studied surface defects after the EPol treatment (Fig. 7). Since these irregularities are mainly observed in the magnesium alloy, it can be assumed that secondary phases or inclusions have been dissolved from the material during electropolishing, resulting in shallow dents on the surface. Since these inclusions are irregularly distributed on the surface, this would also explain the significant variations between the S_z measurements of electropolished AM50 surfaces (Fig. 6b). Nevertheless, the observed formation of gas bubbles during electropolishing should also be considered. It is assumed that oxygen is produced at the metal anode via a special mechanism with prior formation of OH radicals [27]. In this context, the interplay of rising gas bubbles and the sinking electrolyte loaded with metal ions can lead to various structures and waviness on the sample surface. At low current density, the bubbles even remain attached to the surface due to their low buoyancy [27]. Due to the flat, round shape of the surface defects, pitting is excluded. As it was very difficult to see the defects on surface images, it should be mentioned that CLSM is an appropriate measuring instrument for detecting this kind of surface defect. The small pits found in pure magnesium could be pores in the material.

4.4. Corrosion rates

The corrosion rates of electropolished magnesium materials were determined using potentiodynamic polarisation. The cell culture medium DMEM was chosen as electrolyte because the composition and buffering system are similar to those of blood plasma [49,50]. The analysis of the electrochemical results (Fig. 9 and Table 3) revealed that electropolishing leads to the lowest corrosion rate (0.08 mm·year^{-1}) of magnesium materials among the considered surface treatments. The effect of an improved corrosion behaviour after electropolishing was also observed with the common electropolishing metals, like stainless steel, in other studies [24,51–53]. A comparison of the determined corrosion rates after electropolishing with literature data is difficult due to the lack of investigations of the corrosion behaviour of electropolished magnesium materials. However, since for example Hornberger et al. [9] noted for untreated pure magnesium a corrosion rate of 0.6 mm·year^{-1}, the corrosion data of electropolished magnesium materials obtained in this study show that electropolishing can give an important contribution to the corrosion control of magnesium materials. In addition, the fact that in vitro degradation tends to be higher than in vivo [2], even lower corrosion rates can be expected.

In general, there are several reasons for the increased corrosion stability after electropolishing. One factor, which can influence the rate of the corrosion process, is the surface roughness of the magnesium materials. However, due to opposite results, this parameter is considered controversial in the literature. Nguyen et al. [54] indicated an increase

in corrosion resistance due to smoother surfaces, while Alvarez et al. [55] observed a declined corrosion stability with reduced surface roughness. In this context, the results in Figs. 6 and 9 show, that electropolished and mechanically polished surfaces achieved similarly low S_a-values of approx. 0.05 µm, however, the corrosion rate after electropolishing (0.08 mm·year^{-1}) and after mechanical polishing (1.54 mm·year^{-1}) differ significantly by a factor of almost 20. Therefore, the process type must take a decisive role for the observed corrosion behaviour.

On the one hand, electropolishing leads to a removal of the outermost surface layer, ion by ion. This layer is usually plastically deformed and contains structural defects of manufacturing or mechanical pretreatments as well as corrosion-susceptible components, which are the causes of increased electrochemical activity of the surface [21]. On the other hand, it can be assumed that a new oxide layer is formed on the surface after electropolishing, which is more stable and homogeneous and consequently protects the magnesium material better against corrosive attack as found in stainless steel [21,24]. Using Raman spectroscopy bands of MgO and $Mg(OH)_2$ could be detected, however the peak of measured MgO on the electropolished surface cannot be distinguished from that on the ground surface. It is possible that the oxide layer formed after electropolishing is more uniform, more defect-free or even thicker. A different oxide composition or bonding is also conceivable as phosphate was detected in the electropolished surfaces. Furthermore, from microhardness measurements, it was concluded that electro polishing leads to a reduced density of dislocations and twinning. That may also contribute to increase corrosion resistance since dislocations and twinning are lattice defects. Therefore, further investigations should be carried out in the future to obtain more information in this topic. In this context, X-ray photoelectron spectroscopy (XPS[20]) can determine the chemical composition of the oxide layer more precisely, ellipsometry can measure the thickness of the oxide layer, and using TEM dislocations and twinning can studied.

The presence of 10% FBS in DMEM is a routine addition for corrosion tests [49] and leads to lower corrosion rates (Fig. 9) due to the interaction of the protein-containing electrolyte with the absorbable material [45]. However, electropolished samples exhibit in DMEM and DMEM+FBS similar corrosion rates, indicating that proteins are less able to adhere to electrochemically treated surfaces. In this context, Awad et al. [56] noted that also bacteria have problems adhering to electropolished surfaces. A second hypothesis would be that the proteins can adhere to electropolished surfaces, but their influence is no longer decisive because the corrosion rate has already been reduced to a minimum by electropolishing.

4.5. Corrosion mechanism and products

Despite improved corrosion rates after electropolishing, electrochemically treated magnesium surfaces still show localised corrosion modes. The corroded sites are inhomogeneous pits in the surface that spread at different rates (Fig. 11) and a typically increased Cl-concentration (Fig. 12) can be measured within the corrosion sites. This indicates that the oxide layer formed after electropolishing became still locally unstable due to the high content of Cl in DMEM and developed into more soluble $MgCl_2$, promoting the dissolution of magnesium [3,8]. However, a slowdown in corrosion after electropolishing can also be observed when examining the corroded surface areas. Compared to mechanically and chemically treated samples, the measuring area of the minicell cannot be seen as corroded circle on electropolished surfaces (Fig. 10). A qualitative estimation also suggests that electropolished samples indicate a lower number of pits on the surface. As a result, it can be assumed that the surface was better protected against corrosion by electropolishing and consequently exhibits a higher corrosion resistance than the mechanically and chemically treated surfaces. The composition of the formed corrosion products depends on the used electrolyte solution [50]. In addition to Cl, traces of Ca and K, which are all components of the electrolyte DMEM, could be detected within the corrosion sites of electropolished samples.

4.6. Further surface properties

Regarding other surface properties, it can be assumed that electropolished magnesium materials exhibit a higher wettability than the otherwise treated surfaces. This can be interpreted from the measured contact angles. For both, water and body-like liquid, a contact angle of approx. 25–35° can be noted for AM50 and pure magnesium, which, as expected, is associated with a high surface energy. The improved wetting behaviour can be explained by the removal of surface contaminations after electropolishing [21,25]. Further investigations using XPS can show, which contaminations, presumably carbon contaminations, have been removed. For practical applications, it can be assumed that a wettable surface leads to a more even distribution of body-like fluids on the magnesium component, so that the corrosive attack can also occur more uniform. Latifi et al. [25] also noted more hydrophilic surfaces when electrochemically polishing of 316 L.

The study of microhardness showed that electropolished magnesium materials have a lower Vickers hardness than ground and pickled surfaces. Values of approx. 50 HV 0.1 were achieved for AM50, whereas ground samples were up to 80 HV 0.1. The high microhardness after mechanical grinding can be explained due to residual surfaces stresses induced by the strong plastic deformation and increased dislocation and twinning density in the surface layer during grinding [21]. As already mentioned, the deformed top surface layer is removed during material dissolution by electropolishing, which consequently leads to a reduction in surface hardness and could also result in an improved corrosion behaviour.

5. Conclusion

This characterisation study of electropolished magnesium materials was performed with the purpose of demonstrating three aspects: (1) the suitability of magnesium and its alloys for electropolishing, (2) an appropriate electropolishing process for magnesium materials and (3) the improvement of various surface properties of magnesium by using electropolishing. The chosen experimental conditions (phosphoric acid and ethanol as electropolishing electrolyte, voltage of 4 V, polishing time of 10 min) resulted in bright, structure-less and microscopically smooth surfaces. Moreover, electropolished magnesium materials exhibit less surface stresses as well as higher wettability compared to the other tested surface treatments. One of the most important advances, however, is the increased corrosion resistance after electropolishing, demonstrated by potentiodynamic polarisation. The localised corrosion mode could be reduced, but not entirely prevented. Overall, the electrochemical method indicates great potential to establish as suitable post-treatment procedure for magnesium-based components. Due to the complexity of the degradation process, further test methods (like immersion tests, impedance spectroscopy) are recommended to obtain more information about the corrosion behaviour in physiological environments as well as in the long term. In addition, the effects of the interaction between the individual components of the microstructure and the polishing process must be investigated in more detail. From a biomedical point of view, it would be of interest to transfer the presented electropolishing process to medically relevant magnesium materials, such as WE43, in the next step.

Funding

This research received no external funding.

CRediT authorship contribution statement

Sarau George: Resources. **Sotelo Lamborghini:** Investigation.

Schultheiß Ulrich: Investigation, Methodology, Writing – review & editing. **Kloiber Jessica:** Conceptualization, Data curation, Formal analysis, Investigation, Methodology, Validation, Visualization, Writing – original draft. **Hornberger Helga:** Conceptualization, Funding acquisition, Methodology, Project administration, Resources, Supervision, Validation, Writing – review & editing. **Hort Norbert:** Resources. **Gavras Sarkis:** Investigation, Writing – review & editing. **Christiansen Silke:** Resources.

Declaration of Competing Interest

The authors declare that they have no known conflict of interest, for example the validity of our research is not be influenced by a secondary interest, such as financial gain.

Data availability

Data will be made available on request.

Acknowledgements

The authors gratefully thank Regensburg Centre of Biomedical Engineering (RCBE) for providing laboratory consumables. They also thank Prof. Dr. Ing. Ulf Noster for providing the laboratory and equipment for electropolishing and Dr. rer. nat. Brigit Striegl for supporting in chemical questions and in the evaluation of the Raman data.

G.S. and S.C. were funded by the European Union within the research projects 4D+nanoSCOPE and LRI C10 and by the "Freistaat Bayern" and European Union within the project „Analytiktechnikum für Gesundheits- und Umweltforschung - AGEUM", StMWi-43–6623-22/1/3. L.S. is directly funded by the European Union's H2020 research and innovation programme under the Marie Sklodowska-Curie grant agreement AIMed no.861138, 2020–2023.

Appendix A. Supporting information

Supplementary data associated with this article can be found in the online version at doi:10.1016/j.mtcomm.2023.107983.

References

[1] P. Chakraborty Banerjee, S. Al-Saadi, L. Choudhary, S.E. Harandi, R. Singh, Magnesium implants: prospects and challenges, Materials 12 (2019) 136, https://doi.org/10.3390/ma12010136.
[2] A.H.Martinez Sanchez, B.J.C. Luthringer, F. Feyerabend, R. Willumeit, Mg and Mg alloys: how comparable are in vitro and in vivo corrosion rates? A review, Acta Biomater. 13 (2015) 16–31, https://doi.org/10.1016/j.actbio.2014.11.048.
[3] T. Zhang, W. Wang, J. Liu, L. Wang, Y. Tang, K. Wang, A review on magnesium alloys for biomedical applications, Front. Bioeng. Biotechnol. 10 (2022) 953344, https://doi.org/10.3389/fbioe.2022.953344.
[4] X.-N. Gu, S.-S. Li, X.-M. Li, Y.-B. Fan, Magnesium based degradable biomaterials: a review, Front. Mater. Sci. 8 (2014) 200–218, https://doi.org/10.1007/s11706-014-0253-9.
[5] N.T. Kirkland, Magnesium biomaterials: past, present and future, Corros. Eng. Sci. 47 (2012) 322–328, https://doi.org/10.1179/1743278212Y.0000000034.
[6] H.S. Brar, M.O. Platt, M. Sarntinoranont, P.I. Martin, M.V. Manuel, Magnesium as a biodegradable and bioabsorbable material for medical implants, JOM 61 (2009) 31–34, https://doi.org/10.1007/s11837-009-0129-0.
[7] S. Bahl, S. Suwas, K. Chatterjee, The control of crystallographic texture in the use of magnesium as a resorbable biomaterial, RSC Adv. 4 (2014) 55677–55684, https://doi.org/10.1039/C4RA08484E.
[8] Y. Xin, T. Hu, P.K. Chu, In vitro studies of biomedical magnesium alloys in a simulated physiological environment: a review, Acta Biomater. 7 (2011) 1452–1459, https://doi.org/10.1016/j.actbio.2010.12.004.
[9] H. Hornberger, H. Kissel, B. Striegl, M. Kronseder, F. Vollnhals, S. Christiansen, Bioactivity and corrosion behavior of magnesium barrier membranes, Mater. Corros. 73 (2022) 8–19, https://doi.org/10.1002/maco.202112385.
[10] K. Chen, J. Dai, X. Zhang, Improvement of corrosion resistance of magnesium alloys for biomedical applications, Corros. Rev. 33 (2015) 101–117, https://doi.org/10.1515/corrrev-2015-0007.
[11] X. Li, X. Liu, S. Wu, K.W.K. Yeung, Y. Zheng, P.K. Chu, Design of magnesium alloys with controllable degradation for biomedical implants: from bulk to surface, Acta Biomater. 45 (2016) 2–30, https://doi.org/10.1016/j.actbio.2016.09.005.
[12] I. Marco, A. Myrissa, E. Martinelli, F. Feyerabend, R. Willumeit-Römer, A. M. Weinberg, O. van der Biest, In vivo and in vitro degradation comparison of pure Mg, Mg-10Gd and Mg-2Ag: a short term study, Eur. Cell. Mater. 33 (2017) 90–104, https://doi.org/10.22203/eCM.v033a07.
[13] M. Prakasam, J. Locs, K. Salma-Ancane, D. Loca, A. Largeteau, L. Berzina-Cimdina, Biodegradable materials and metallic implants-a review, J. Funct. Biomater. 8 (2017) 44, https://doi.org/10.3390/jfb8040044.
[14] F. Witte, N. Hort, C. Vogt, S. Cohen, K.U. Kainer, R. Willumeit, F. Feyerabend, Degradable biomaterials based on magnesium corrosion, Curr. Opin. Solid State Mater. Sci. 12 (2008) 63–72, https://doi.org/10.1016/j.cossms.2009.04.001.
[15] R.I.M. Asri, W.S.W. Harun, M. Samykano, N.A.C. Lah, S.A.C. Ghani, F. Tarlochan, M.R. Raza, Corrosion and surface modification on biocompatible metals: a review, Mater. Sci. Eng. C 77 (2017) 1261–1274, https://doi.org/10.1016/j.msec.2017.04.102.
[16] R. Willumeit, J. Fischer, F. Feyerabend, N. Hort, U. Bismayer, S. Heidrich, B. Mihailova, Chemical surface alteration of biodegradable magnesium exposed to corrosion media, Acta Biomater. 7 (2011) 2704–2715, https://doi.org/10.1016/j.actbio.2011.03.004.
[17] S. Gonzalez, E. Pellicer, S. Suriach, M.D. Bar, J. Sort, Biodegradation and mechanical integrity of magnesium and magnesium alloys suitable for implants, in: R. Chamy (Ed.), Biodegradation - Engineering and Technology, InTech, 2013, pp. 313–340.
[18] M. Esmaily, J.E. Svensson, S. Fajardo, N. Birbilis, G.S. Frankel, S. Virtanen, R. Arrabal, S. Thomas, L.G. Johansson, Fundamentals and advances in magnesium alloy corrosion, Prog. Mater. Sci. 89 (2017) 92–193, https://doi.org/10.1016/j.pmatsci.2017.04.011.
[19] H. Hornberger, S. Virtanen, A.R. Boccaccini, Biomedical coatings on magnesium alloys - a review, Acta Biomater. 8 (2012) 2442–2455, https://doi.org/10.1016/j.actbio.2012.04.012.
[20] G. Eddy Jai Poinern, S. Brundavanam, D. Fawcett, Biomedical magnesium alloys: a review of material properties, surface modifications and potential as a biodegradable orthopaedic implant, Am. J. Biomed. Eng. 2 (2013) 218–240, https://doi.org/10.5923/j.ajbe.20120206.02.
[21] W. Han, F. Fang, Fundamental aspects and recent developments in electropolishing, Int. J. Mach. Tools Manuf. 139 (2019) 1–23, https://doi.org/10.1016/j.ijmachtools.2019.01.001.
[22] E.-S. Lee, Machining characteristics of the electropolishing of stainless steel (STS316L), Int. J. Adv. Manuf. Technol. 16 (2000) 591–599, https://doi.org/10.1007/s001700070049.
[23] B. Chatterjee, Science and industry of electropolishing, Galvanotechnik 71 (2015) 77–93.
[24] N. Hassan, N.A. Abdel Ghany, Corrosion of biomaterials: anodic treatment and evaluation of 316L stainless steel in simulated body fluid, Corros. Eng. Sci. Technol. 52 (2017) 267–275, https://doi.org/10.1080/1478422X.2016.1267932.
[25] A. Latifi, M. Imani, M.T. Khorasani, M.D. Joupari, Electrochemical and chemical methods for improving surface characteristics of 316L stainless steel for biomedical applications, Surf. Coat. Technol. 221 (2013) 1–12, https://doi.org/10.1016/j.surfcoat.2013.01.020.
[26] N. Eliaz, O. Nissan, Innovative processes for electropolishing of medical devices made of stainless steels, J. Biomed. Mater. Res. A 83 (2007) 546–557, https://doi.org/10.1002/jbm.a.31429.
[27] M. Buhlert, Elektropolieren - Elektrolytisches Glänzen, Glätten und Entgraten von Edelstahl, Stahl, Messing, Kupfer, Aluminium, Magnesium und Titan, second ed., Leuze, Bad Saulgau; 2017.
[28] A.E.K. Mohammad, D. Wang, Electrochemical mechanical polishing technology: recent developments and future research and industrial needs, Int. J. Adv. Manuf. Technol. 86 (2016) 1909–1924, https://doi.org/10.1007/s00170-015-8119-6.
[29] J. Boban, A. Ahmed, E.K. Jithinraj, M.A. Rahman, M. Rahman, Polishing of additive manufactured metallic components: retrospect on existing methods and future prospects, Int. J. Adv. Manuf. Technol. 121 (2022) 83–125, https://doi.org/10.1007/s00170-022-09382-y.
[30] P.C. Howlett, W. Neil, T. Khoo, J. Sun, M. Forsyth, D.R. MacFarlane, An electrochemical impedance study of ionic liquid film formation and aqueous corrosion of magnesium alloy ZE41, Isr. J. Chem. 48 (2008) 313–318, https://doi.org/10.1560/IJC.48.3-4.313.
[31] J.H.-H. Hung, Y.L. Chiu, T. Zhu, W. Gao, In situ ESEM study of partial melting and precipitation process of AZ91D, Asia-Pac. Jrnl Chem. Eng. 2 (2007) 493–498, https://doi.org/10.1002/apj.87.
[32] R.K. Sabat, S.K. Sahoo, D. Panda, U.K. Mohanty, S. Suwas, Orientation dependent recrystallization mechanism during static annealing of pure magnesium, Mater. Charact. 132 (2017) 388–396, https://doi.org/10.1016/j.matchar.2017.09.003.
[33] H. Ohno, Y. Iizuka, S. Fujita, Pure rotational Raman spectroscopy applied to N_2 /O_2 analysis of air bubbles in polar firn, J. Glaciol. 67 (2021) 903–908, https://doi.org/10.1017/jog.2021.40.
[34] J.P. Singh, L.K. Gupta, Annealing effects on MgO films grown using e-beam evaporation, IJMEMS 4 (2019) 619–626, https://doi.org/10.33889/IJMEMS.2019.4.3-049.
[35] A. Dychalska, P. Popielarski, W. Franków, K. Fabisiak, K. Paprocki, M. Szybowicz, Study of CVD diamond layers with amorphous carbon admixture by Raman scattering spectroscopy, Mater. Sci. 33 (2015) 799–805, https://doi.org/10.1515/msp-2015-0067.
[36] O. Pandoli, R.D.S. Martins, E.C. Romani, S. Paciornik, M.H.D.P. Maurício, H.D. L. Alves, F.V. Pereira-Meirelles, E.L. Luz, S.M.L. Koller, H. Valiente, K. Ghavami, Colloidal silver nanoparticles: an effective nano-filler material to prevent fungal proliferation in bamboo, RSC Adv. 6 (2016) 98325–98336, https://doi.org/10.1039/C6RA12516F.

[37] P.K. Bowen, J. Drelich, J. Goldman, Magnesium in the murine artery: probing the products of corrosion, Acta Biomater. 10 (2014) 1475–1483, https://doi.org/10.1016/j.actbio.2013.11.021.
[38] X. Hu, L. Liu, S. Zhai, The structure-Raman spectra relationships of $Mg_3(PO_4)_2$ polymorphs: a comprehensive experimental and DFT study, Spectrochim. Acta A Mol. Biomol. Spectrosc. 245 (2021) 118906, https://doi.org/10.1016/j.saa.2020.118906.
[39] R. Mahajan, R. Prakash, S. Kumar, V. Kumar, R.J. Choudhary, D.M. Phase, Surface and luminescent properties of $Mg_3(PO_4)_2$:Dy^{3+} phosphors, Optik 225 (2021) 165717, https://doi.org/10.1016/j.ijleo.2020.165717.
[40] T. Athar, A. Hakeem, W. Ahmed, Synthesis of MgO nanopowder via non aqueous sol–gel method, Adv. Sci. Lett. 7 (2012) 27–29, https://doi.org/10.1166/asl.2012.2190.
[41] J. Feng, Y. Chen, X. Liu, T. Liu, L. Zou, Y. Wang, Y. Ren, Z. Fan, Y. Lv, M. Zhang, In-situ hydrothermal crystallization $Mg(OH)_2$ films on magnesium alloy AZ91 and their corrosion resistance properties, Mater. Chem. Phys. 143 (2013) 322–329, https://doi.org/10.1016/j.matchemphys.2013.09.005.
[42] M.H. Zahir, M.M. Rahman, K. Irshad, M.M. Rahman, Shape-stabilized phase change materials for solar energy storage: MgO and $Mg(OH)_2$ Mixed with polyethylene glycol, Nanomaterials 9 (2019) 1773, https://doi.org/10.3390/nano9121773.
[43] S. Burikov, T. Dolenko, S. Patsaeva, Y. Starokurov, V. Yuzhakov, Raman and IR spectroscopy research on hydrogen bonding in water-ethanol systems, Mol. Phys. 108 (2010) 2427–2436, https://doi.org/10.1080/00268976.2010.516277.
[44] K.B. Hensel, Electropolishing, Met. Finish. 100 (2002) 425–433, https://doi.org/10.1016/S0026-0576(02)82046-3.
[45] I. Johnson, W. Jiang, H. Liu, The effects of serum proteins on magnesium alloy degradation in vitro, Sci. Rep. 7 (2017) 14335, https://doi.org/10.1038/s41598-017-14479-6.
[46] P. Lochyński, S. Charazińska, E. Łyczkowska-Widłak, A. Sikora, Electropolishing of stainless steel in laboratory and industrial scale, Metals 9 (2019) 854, https://doi.org/10.3390/met9080854.
[47] G. Yang, B. Wang, K. Tawfiq, H. Wei, S. Zhou, G. Chen, Electropolishing of surfaces: theory and applications, Surf. Eng. 33 (2017) 149–166, https://doi.org/10.1080/02670844.2016.1198452.
[48] N. Li, Y. Zheng, Novel magnesium alloys developed for biomedical application: a review, J. Mater. Sci. Technol. 29 (2013) 489–502, https://doi.org/10.1016/j.jmst.2013.02.005.
[49] Di Mei, S.V. Lamaka, X. Lu, M.L. Zheludkevich, Selecting medium for corrosion testing of bioabsorbable magnesium and other metals – a critical review, Corros. Sci. 171 (2020) 108722, https://doi.org/10.1016/j.corsci.2020.108722.
[50] J. Gonzalez, R.Q. Hou, E.P.S. Nidadavolu, R. Willumeit-Römer, F. Feyerabend, Magnesium degradation under physiological conditions - best practice, Bioact. Mater. 3 (2018) 174–185, https://doi.org/10.1016/j.bioactmat.2018.01.003.
[51] S.-J. Lee, J.-J. Lai, The effects of electropolishing (EP) process parameters on corrosion resistance of 316L stainless steel, J. Mater. Process. Technol. 140 (2003) 206–210, https://doi.org/10.1016/S0924-0136(03)00785-4.
[52] Z. ur Rahman, K.M. Deen, L. Cano, W. Haider, The effects of parametric changes in electropolishing process on surface properties of 316L stainless steel, Appl. Surf. Sci. 410 (2017) 432–444, https://doi.org/10.1016/j.apsusc.2017.03.081.
[53] S. Habibzadeh, L. Li, D. Shum-Tim, E.C. Davis, S. Omanovic, Electrochemical polishing as a 316L stainless steel surface treatment method: towards the improvement of biocompatibility, Corros. Sci. 87 (2014) 89–100, https://doi.org/10.1016/j.corsci.2014.06.010.
[54] T.L. Nguyen, A. Blanquet, M.P. Staiger, G.J. Dias, T.B.F. Woodfield, On the role of surface roughness in the corrosion of pure magnesium in vitro, J. Biomed. Mater. Res. B 100B (2012) 1310–1318, https://doi.org/10.1002/jbm.b.32697.
[55] R.B. Alvarez, H.J. Martin, M.F. Horstemeyer, M. Chandler, N. Williams, P.T. Wang, A. Ruiz, Corrosion relationships as a function of time and surface roughness on a structural AE44 magnesium alloy, Corros. Sci. 52 (2010) 1635–1648, https://doi.org/10.1016/j.corsci.2010.01.018.
[56] A.M. Awad, E.A. Ghazy, S.A. Abo El-Enin, M.G. Mahmoud, Electropolishing of AISI-304 stainless steel for protection against SRB biofilm, Surf. Coat. Technol. 206 (2012) 3165–3172, https://doi.org/10.1016/j.surfcoat.2011.11.046.